FRONTIERS OF PHYSICS

RESEARCH ARTICLE
Volume 18 / Issue 6 / 63303 / 2023

# Freeze-drying assisted liquid exfoliation of $BiFeO_3$ for pressure sensing

Yuping Li, Mengwei Dong, Xuejie Zou, Jinhao Zhang, Jian Zhang†, Xiao Huang‡

Key Laboratory of Flexible Electronics (KLOFE) & Institute of Advanced Materials (IAM), Jiangsu National Synergetic Innovation Center for Advanced Materials (SICAM), Nanjing Tech University (NanjingTech), 30 South Puzhu Road, Nanjing 211816, China
Corresponding authors. E-mail: †iamjzhang@njtech.edu.cn, ‡iamxhuang@njtech.edu.cn
Received December 11, 2022; accepted April 24, 2023



## ABSTRACT

Breaking up bulk crystals of functional materials into nanoscale thinner layers can lead to interesting properties and enhanced functionalities due to the size and interface effects. However, unlike the van der Waals layered crystals, many materials cannot be exfoliated into thin layers by liquid exfoliation. $BiFeO_3$ is a piezoelectric ceramic material, which is commonly synthesized as bulk crystals, limiting its wider applications. In this contribution, a freeze-drying assisted liquid exfoliation method was adopted to fabricate thin-layered $BiFeO_3$ nanoplates with lateral sizes of up to 500 nm and thicknesses of 10–20 nm. The freeze-drying process showed a vital role in the preparation process by imposing stress on the dispersed $BiFeO_3$ crystals during the liquid-to-solid-to-gas transition of the solvent. Such stress resulted in lattice strains in the freeze-dried $BiFeO_3$ crystals, which enabled their further exfoliation under subsequent ultrasonication. Considering the intrinsic piezoelectric effect of $BiFeO_3$, pressure sensors based on bulk and thin-layer $BiFeO_3$ were also fabricated. The pressure sensor based on $BiFeO_3$ nanoplates exhibited a largely enhanced sensitivity with a wider working range than the bulk counterpart, because of the stronger piezoelectric effect induced and the extra electrical charges at abundant interlayer interfaces. We suggest that the freeze-drying assisted liquid exfoliation method can be applied to other non-van der Waals crystals to bring about more functional material systems.

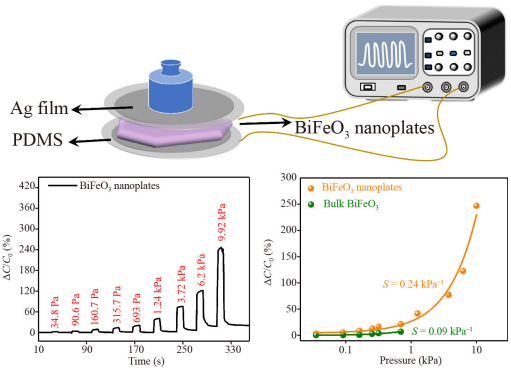


**Keywords** $BiFeO_3$ nanoplates, liquid exfoliation, piezoelectricity, pressure sensor

## 1 Introduction

Pressure sensors are gaining tremendous attention due to their applications in wearable sensing devices [1, 2], medical diagnosis [3, 4], electronic skins (e-skin) [5, 6], and soft touch displays [7, 8]. On the basis of the transduction mechanism, pressure sensors can be divided into the piezoresistive type [9], capacitance type [10], and piezoelectric type [11]. Among them, the piezoelectric-type pressure sensors, which rely on the generation of electrical charges in solid materials in response to an applied mechanical pressure, have received special attention because of their high sensitivity and fast response

#Special Topic: Two-dimensional Electronic Materials and Devices (Eds.: Lin Wang & Xiaolong Chen).

Higher Education Press

https://doi.org/10.1007/s11467-023-1301-7

[12, 13]. Till now, various piezoelectric materials, including polymeric materials [14], inorganic semiconductors [15] and ceramics [16], were employed for the fabrication of piezoelectric devices. Compared with inorganic semiconductors and piezoceramic, piezoelectric polymer materials are flexible and can sustain larger mechanical strains but with the lower piezoelectric coefficient [17–19].

As a kind of piezoelectric ceramic materials, $BiFeO_3$ has attracted increasing attention since the discovery of $BiFeO_3$ thin film with a remnant ferroelectric polarization [20]. $BiFeO_3$ has a rhombohedral twisted crystal structure, in which the hybridization between $Bi^{3+}$ lone pairs (6s orbital) and $O^{2-}$ (2p orbital) results in a displacement of $Bi^{3+}$ from a centrosymmetric position, resulting in high spontaneous polarization [21]. It was demonstrated that $BiFeO_3$ exhibited high multiferroic properties over a wide temperature range. However, mostly reported bulk $BiFeO_3$ ceramics showed limited piezoelectric properties due to leakage problems [22]. Piezoelectricity is the ability of a material to generate an internal electric field when subjected to mechanical stress, which is largely depended on the thickness [23] and crystal structure of the material [24], as well as the magnitude of epitaxial strain [25, 26]. It was reported that piezoelectric materials with a multilayer structure exhibited an improved piezoelectric output, attributing to the electric capacity enhancement of the double-layered structure [27]. Moreover, DFT calculation of the piezoelectric coefficients of monolayer transition metal dichalcogenides indicated that some of them exhibited stronger piezoelectric coupling than traditionally employed bulk structures [28]. Therefore, there is a reason to believe that the piezoelectric properties of bulk $BiFeO_3$ crystals could be improved by breaking them into thinner layers. $BiFeO_3$ has a layered crystal structure, where the bismuth ions are distributed above and below the ferrite octahedron and share a common edge. A previous theoretical work predicted that the vertical repulsion of bismuth atoms between the layers might make the exfoliation of bulk $BiFeO_3$ become possible [29]. Unfortunately, unlike with van der Waals layered materials whose interlayer interaction can be easily overcome, direct liquid phase exfoliation of $BiFeO_3$ into thin nanoplates/nanosheets remains challenging.

In this study, thin-layer $BiFeO_3$ nanoplates were prepared by a hydrothermal method followed by a freeze-drying assisted liquid exfoliation process for the first time. The liquid exfoliation mechanism was detailed by changing the exfoliation solvent and ultrasonication time. The as-exfoliated $BiFeO_3$ nanoplates with optimized conditions showed lateral sizes of 400–500 nm with thicknesses of 10–20 nm. As a proof of concept demonstration, pressure sensors based on the $BiFeO_3$ nanoplates exhibited largely enhanced pressure response, which is nearly 5 times higher than that of bulk $BiFeO_3$ crystals under an applied pressure of 693 Pa, attributing to interface effect enhanced piezoelectric property.

## 2 Experiments

### 2.1 Materials

Bismuth nitrate pentahydrate ($Bi(NO_3)_3{\cdot}5H_2O$, > 99%) was purchased from Adamas (Shanghai, China). Ferric chloride hexahydrate ($FeCl_3{\cdot}6H_2O$) and sodium hydroxide (NaOH, > 99%) were purchased from Innochem (Beijing, China). Ethanol (anhydrous, > 99.7%), methanol (anhydrous, > 99.9%), and acetone (anhydrous, > 99.7%) were purchased from Shanghai Chemical Reagent Co., Ltd (Shanghai, China). The main agent and curing agent of polydimethylsiloxane (PDMS) were purchased from Sylgard (Suzhou, China). All the materials were used without further purification.

### 2.2 Synthesis of bulk $BiFeO_3$ crystals

The raw materials, $[Bi(NO_3)_3{\cdot}5H_2O]$ and $[FeCl_3{\cdot}6H_2O]$ with a stoichiometric molar ratio of 1:1 were dissolved in acetone and distilled water with a volume ratio of 3:10 by continuous stirring until the formation of a clear solution. Then, 13 M ammonia hydroxide solution was added until the pH of the mixed solution reached 11–12. The obtained sediment by centrifugation was washed with distilled water for several times until the pH of the liquid supernatant was 7.0. Afterwards, the sediment was re-dispersed into 5 M NaOH solution and stirred for 30 min. Then, the mixed solution was transferred to a sealed Teflon-lined steel autoclave and heated at 140 °C for 12 h. The as-prepared black powder ($BiFeO_3$) was transferred to 3 mL 4 M $HNO_3$ and stirred for 8 h to remove impurities.

### 2.3 Freeze-drying assisted liquid exfoliation of bulk $BiFeO_3$

The $BiFeO_3$ powder was dispersed in 2 mL methanol and freeze dried in liquid nitrogen. Afterwards, 0.046 mg freeze-dried powder was re-dispersed in 3 mL methanol and ultrasonicated in a water bath for 8 h at room temperature. Subsequently, the extracted upper suspension was washed by methanol for three times to obtain thin $BiFeO_3$ nanoplates.

### 2.4 Fabrication of $BiFeO_3$ nanoplate-based pressure sensors

First, the elastomer and curing agent of PDMS (mass ratio = 10:1) were mixed thoroughly and then degassed under vacuum to remove air bubbles. This mixture was then poured into a mold with a thickness of 1 millimeter and cured at 80 °C for 1 h to prepare a PDMS thin film.

A copper wire was fixed on the surface of the PDMS film by using conductive silver glue. Two of such films were used as the top and bottom electrodes of a pressure sensor. Finally, pressed $BiFeO_3$ nanoplates was placed between the two parallel electrodes.

### 2.5 Characterization

The samples were characterized with a scanning electron microscopy (SEM JEOL JSM-7800F, Japan), a transmission electron microscope (TEM JEOL 2100 F, Japan), a high-resolution transmission electron microscope (HRTEM JEOL 2100 Plus, Japan), an atomic force microscope (AFM, MultiMode8, Bruker), an X-ray diffractometer (XRD, SmartLab Rigaku, Japan) with Cu Kα radiation at $\lambda = 1.54$ Å, a LabRAM HR Evolution Raman spectrometer (Horiba Jobin Yvon) with a 532 nm laser focused through a 100× objective lens, a polar device (PZT-JH10/4, China) and Hydrostatic electric coefficient ($d_{33}$) measuring instrument (ZJ-3, China).

## 3 Results and discussion

### 3.1 The morphology and microstructure of $BiFeO_3$ nanoplates

Figure 1(a) shows the schematic diagram of the preparation process for $BiFeO_3$ nanoplates. Bulk $BiFeO_3$ was prepared by a hydrothermal coprecipitation method with $Bi(NO_3)_3{\cdot}5H_2O$ and $FeCl_3{\cdot}6H_2O$ as precursors. $BiFeO_3$ nanoplates were obtained by combining a freeze-drying process and a following liquid exfoliation process. As shown in the scanning electron microscopy (SEM) and transmission electron microscopy (TEM) images in Figs. 1(b) and (c), the bulk $BiFeO_3$ crystals showed large sizes of 1–2 μm, while the as-exfoliated $BiFeO_3$ nanoplates show lateral sizes of 400 to 500 nm with thicknesses of 10–20 nm (Fig. S1). The phase structures of the $BiFeO_3$ crystals before and after exfoliation were determined by XRD. As shown in Fig. 1(d), well-defined XRD peaks assignable to (012), (110), (006), (202), and (211) planes of $BiFeO_3$ (JCPDS No.71-2494) can be clearly observed in both samples. The high resolution TEM (HRTEM) image [Fig. 1(e)] of an as-exfoliated $BiFeO_3$ nanoplate shows interplanar distances of 0.28 nm and 0.23 nm which can be assigned to (110) and (006) planes of $BiFeO_3$, respectively, suggesting the successful exfoliation of bulk $BiFeO_3$ by freeze-drying assisted liquid exfoliation method. Moreover, the Raman spectra of bulk $BiFeO_3$ and $BiFeO_3$ nanoplates in Fig. S2 both show characteristic modes of E-1, $A_1$-1 and $A_1$-2 at 75 $cm^{-1}$, 152.6 $cm^{-1}$ and 177.5 $cm^{-1}$, respectively, further confirming the phase purity of the as-prepared samples [30].

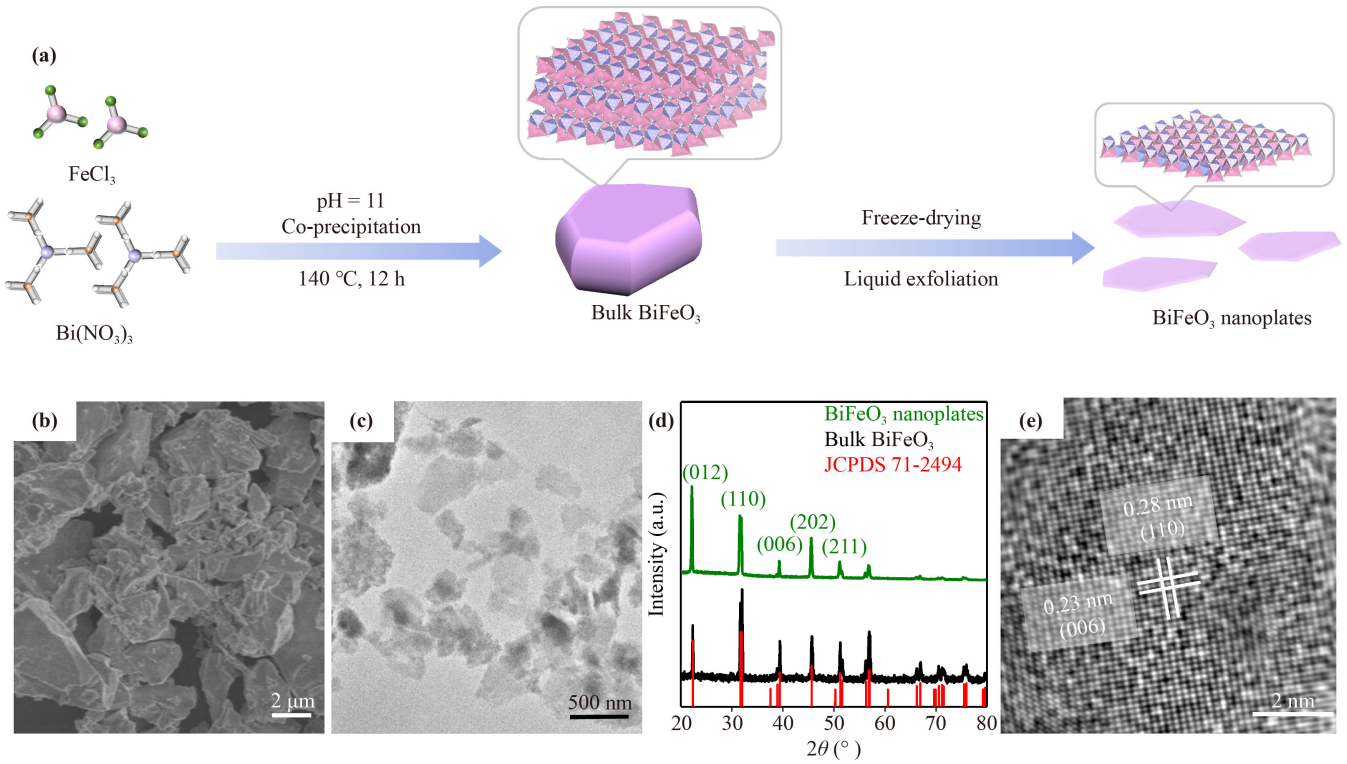


**Fig. 1** **(a)** Schematic diagram of preparation process for thin-layer $BiFeO_3$ nanoplates. **(b)** SEM image of bulk $BiFeO_3$ crystals. **(c)** TEM image of as-exfoliated thin-layer $BiFeO_3$ nanoplates. **(d)** XRD patterns of the bulk $BiFeO_3$ and as-exfoliated $BiFeO_3$ nanoplates. **(e)** HRTEM image of an as-exfoliated $BiFeO_3$ nanoplate.

### 3.2 The formation mechanism of thin-layer $BiFeO_3$ nanoplates by exfoliation

As described above, the $BiFeO_3$ nanoplates were successfully prepared by a freeze-drying assisted liquid exfoliation method. Here, to detail the whole formation mechanism, the effect of freeze-drying process during exfoliation was explored. Without the freeze-drying process, $BiFeO_3$ crystals treated under the same ultrasonication condition showed much thicker morphology as shown in Fig. S3, indicating that the freeze-drying process is an important step in the whole exfoliation process. We first examined the morphologies of the $BiFeO_3$ crystals before freeze-drying and after freeze-drying with different solvents, and found no obvious morphological changes (Fig. S4). We therefore compared their XRD patterns [Fig. 2(a), Fig. S5]. Interestingly, their XRD peaks shift slightly to lower angle after freeze-drying, and the amount of shift is the largest when methanol was used as the solvent for freeze-drying. This suggests that the liquid to solid and then to gas transition of the solvent during freeze-drying can pose stress on the dispersed crystals, and cause lattice strain in them. This agrees with previous reports that freeze-drying was employed to weaken the van der Waals force in layered crystals [31–33]. As shown in Fig. 2(b), our work demonstrates that the freeze-drying can also induce strain in non-van der Waals crystals such as $BiFeO_3$. The reason why the freeze-drying process with methanol as the solvent led to the largest lattice strain might be due to the larger volume change of methanol during liquid-to-solid transition as compared to water and ethanol (Table 1). Such a large strain helps further break up the crystals into thinner nanoplates under subsequent ultrasonication.

After confirming the important role of the freeze-drying process, the effect of the subsequent liquid exfoliation conditions, i.e., the ultrasonication time and solvents were then analyzed. In these control experiments, $BiFeO_3$ crystals treated by the optimized freeze-drying condition with methanol as the solvent were used as the starting material. Figure 3 shows the XRD patterns and TEM images of products obtained after ultrasonication in water, ethanol and methanol for 8 h. Interestingly, the XRD peaks all shift to lower angles (Fig. S6), suggesting further lattice expansion after ultrasonication. The amount of shift is in the order of methanol > water > ethanol. This observation is in line with their morphological difference characterized with

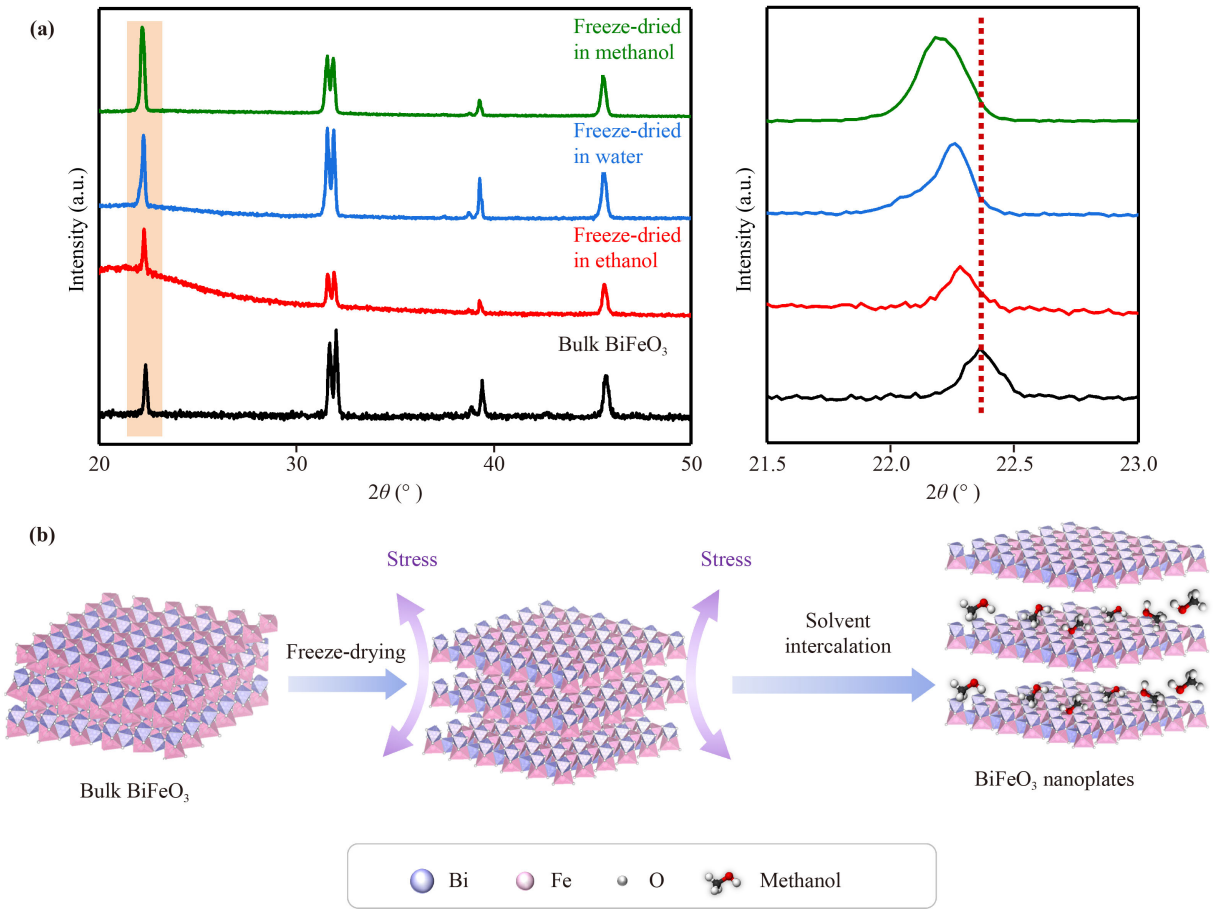


**Fig. 2** **(a)** XRD patterns of bulk $BiFeO_3$ and freeze-dried $BiFeO_3$ in different solvents. **(b)** Schematic illustration of the formation mechanism of $BiFeO_3$ nanoplates.

TEM as shown in Fig. 3(b)–(d). Obviously, the thickness of exfoliated $BiFeO_3$ nanoplates by using methanol is smaller than that of nanoplates exfoliated in water and ethanol. According to the cross-section TEM images in Fig. S7, the thicknesses of typical exfoliated $BiFeO_3$ nanoplates with water and ethanol are 37 and 39 nm, respectively, we further investigated the effect of DMF solvent on the exfoliation and found that the thickness of exfoliated $BiFeO_3$ nanoplates by using DMF (33 nm) as exfoliation solvent in Fig. S8, which indicate the more effective exfoliation with methanol as the solvent. As for the effect of ultrasonication time, it is evident that the exfoliated nanoplates became thinner as the time increased from 4 to 8 h (Figs. S9 and S10).

The reason why methanol is the most effective in facilitating the exfoliation can be explained based on the surface tension and molecular size of the solvent. Compared with water molecules, the surface tension of methanol and ethanol match better with bulk $BiFeO_3$ (Table 1) [34, 35]. However, ethanol has a relatively larger molecule size than methanol, and therefore is more difficult to be inserted inbetween crystal planes of $BiFeO_3$. This is why methanol as the liquid exfoliation solvent owns the better exfoliation ability compared to ethanol with the larger molecule size or water with the unmatchable surface tension [36].

### 3.3 The sensing performance of $BiFeO_3$ nanoplates/PDMS based pressure sensor

As a demonstration, the exfoliated $BiFeO_3$ nanoplates were fabricated into a pressure sensor to measure pressures from 34.8 Pa to 9.9 kPa [Fig. 4(a)]. For comparison, the bulk $BiFeO_3$ based pressure sensor was also fabricated,

**Table 1** Volume change during liquid-to-solid transition and surface tension of the different solvents.

| Solvent | Liquid density (g/cm$^3$) | Solid density (g/cm$^3$) | Volume change (%) | Surface tension (mN/m) |
|---|---|---|---|---|
| Methanol | 0.791 | 0.899 | –12.02 | 21.82 |
| Ethanol | 0.789 | 0.848 | –6.02 | 21.33 |
| Water | 1.0 | 0.92 | 8.7 | 71.12 |

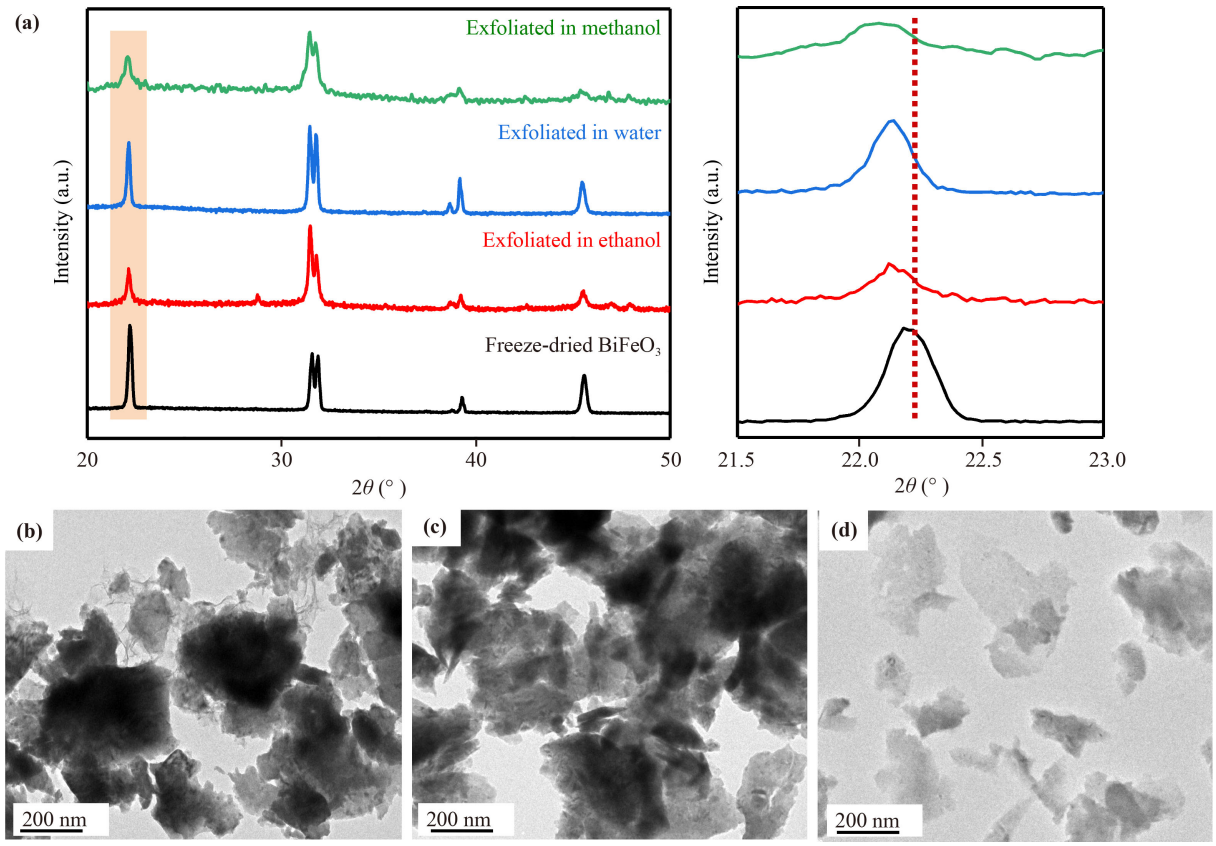


**Fig. 3** **(a)** XRD patterns of freeze-dried bulk $BiFeO_3$ and products obtained after exfoliation in ethanol, water and methanol. TEM images of products obtained after exfoliation in **(b)** ethanol, **(c)** water and **(d)** methanol for 8 h.

but showed a narrower working range that the sensing film was fractured when the pressure exceeded 693 Pa. The fracture of sensing film is closely associated with the intrinsic stress during the fabrication process. In analogy, with the flexible characteristics of two-dimensional materials, exfoliated thin-layer $BiFeO_3$ nanoplate tend to have the decreased intrinsic stress, which can withstand the larger external pressures compared to bulk $BiFeO_3$ crystal [37]. Figure 4(b) shows their responses to varying pressures over the range from 34.8 Pa and 693 Pa. The sensor response is defined by $\Delta C/C_0$, where $C_0$ is the initial capacitance and $\Delta C$ is the capacitance variation under an external pressure. The sensitivity was defined by $(\Delta C/C_0 \times 100\%)/\Delta P$, where $\Delta P$ is the variation of pressure, The $BiFeO_3$ nanoplate based sensor showed up to five times of increased responses as compared to the sensor based on bulk $BiFeO_3$ in the lower pressure range. The sensitivity of the two types of sensors were further calculated by fitting their response-pressure curves, as shown in Fig. 4(c). the bulk $BiFeO_3$ sensor showed a sensitivity of 0.09 $kPa^{-1}$ in the range of 34.8–693 Pa, while the sensor based on $BiFeO_3$ nanoplates presented an improved sensitivity of 0.24 $kPa^{-1}$ in the range of 34.8 Pa–9.9 kPa, and the sensor response reached 250% at 9.9 kPa. Besides, the durability of our sensor based on $BiFeO_3$ nanoplates was evaluated by sensing tests under repeated loading of 34.8 Pa and 251.5 Pa pressure. As shown in Fig. 4(d), the sensor exhibited stable sensing responses without obvious degradation after more than 40 cycles, suggesting a good stability.

The enhanced pressure sensing property of $BiFeO_3$ nanoplates can be explained based on the interface effect promoted piezoelectricity. The piezoelectric effect is the ability of a piezoelectric material to generate an electric field in response to an applied mechanical stress [38]. A material's piezoelectric coefficient ($d_{33}$) is defined by $\mathrm{d}Q/\mathrm{d}F = (U\mathrm{d}C + C\mathrm{d}U)/\mathrm{d}F$, where $\mathrm{d}Q$ is the variation of electric charge, $\mathrm{d}F$ is the variation of external force, $\mathrm{d}C$ is the variation of capacitance and $\mathrm{d}U$ is the variation of voltage [39]. When the voltage and applied force are given, the $d_{33}$ value is directly proportional to changes in capacitance. Therefore, the sensitivity of the capacitance-based pressure sensor increases with increasing piezoelectric effect. The piezoelectric property of a material depends on its atomic orientation, size and edge types. Generally, the bond breaking of edge parts can lead to

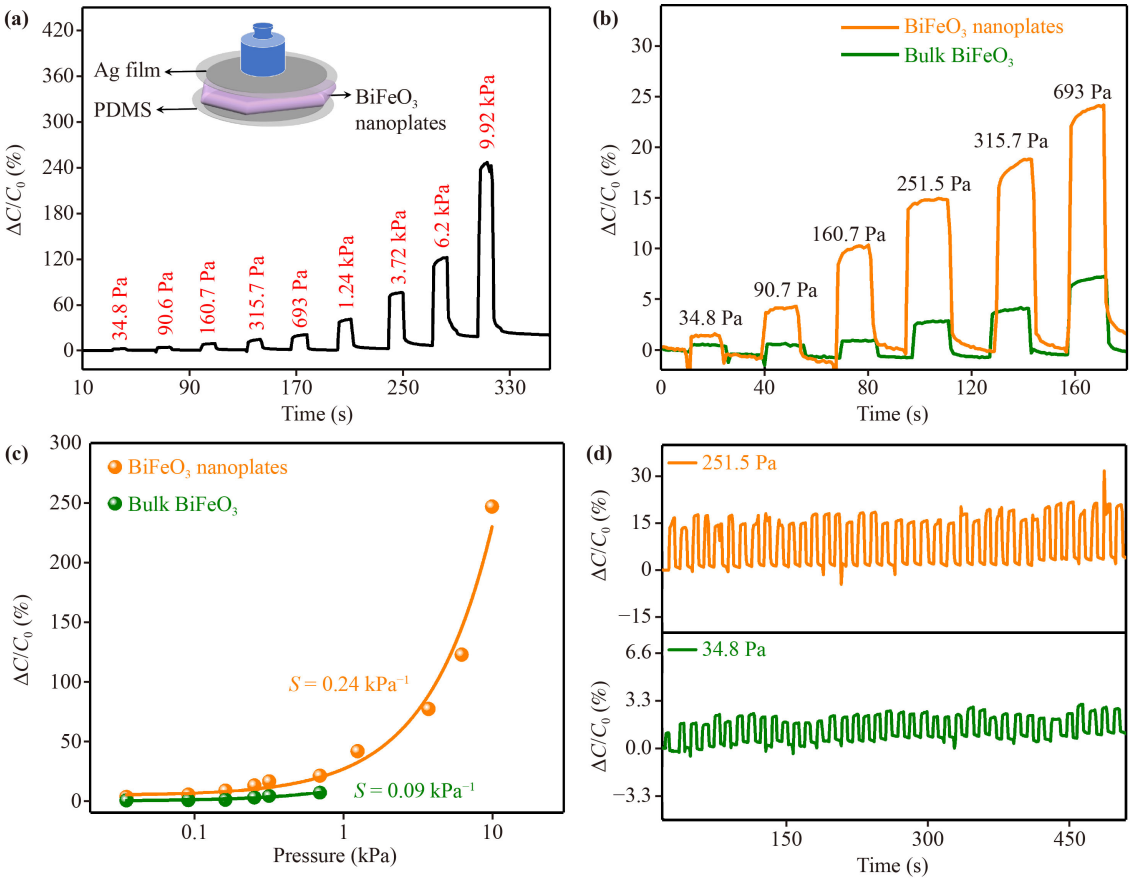


**Fig. 4** **(a)** The response of a pressure sensor based on thin-layer $BiFeO_3$ nanoplates under an applied pressure range of 34.8 Pa–9.9 kPa. **(b)** Comparison of the responses of sensors based on nanoplates and bulk crystals of $BiFeO_3$ under an applied pressure range of 34.8–693 Pa. **(c)** Pressure-response curves of sensors based on nanoplates and bulk crystals of $BiFeO_3$. **(d)** Long-term stability of sensor based on $BiFeO_3$ nanoplates under 34.8 Pa and 251.5 Pa pressure.

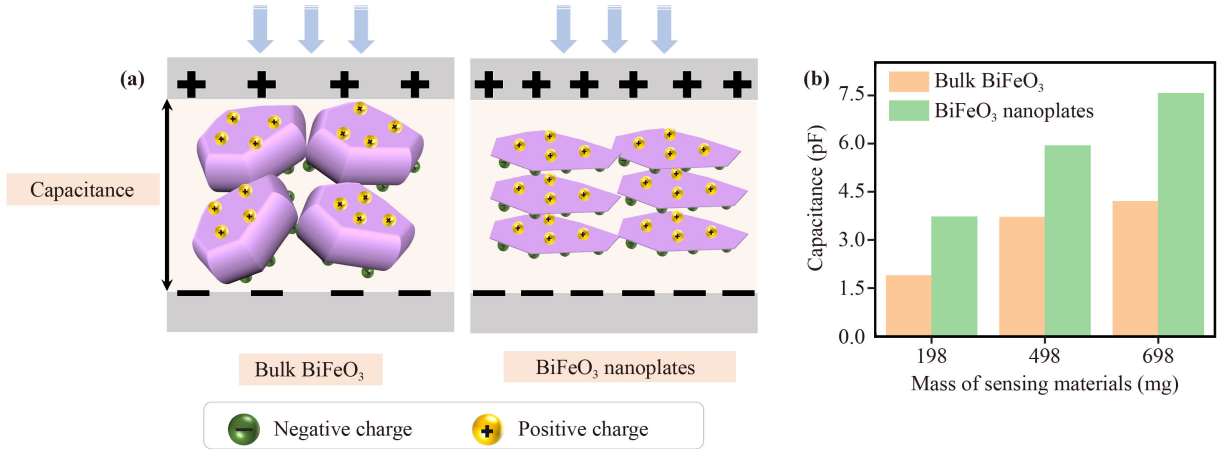


**Fig. 5** **(a)** Schematic illustration of the sensing mechanism of bulk and thin-layer $BiFeO_3$ based pressure sensor. **(b)** The plot between the capacitance and mass of sensing material.

the relaxation of bond identities, including bond length and strength, which significantly influence the related piezoelectric properties of the system [40]. Based on the XRD patterns of $BiFeO_3$ crystals before and after exfoliation, the bond breaking process along with lattice expansion was also involved during the exfoliation process. From their TEM images we can see that the exfoliated nanoplates showed irregular edges, suggesting that the exposed facet/edge types are random and some of them are probably different from those of bulk crystals. These changes of exposed facet/edge types and the increased amount of exposed surfaces can lead to the change of piezoelectric coefficient ($d_{33}$) [41, 42]. We further measured $d_{33}$ of bulk $BiFeO_3$ crystals and exfoliated $BiFeO_3$ nanoplates as shown in Table S1. It was found that the coefficient of exfoliated $BiFeO_3$ nanoplates (5.6 pC/N) was two times higher than that of bulk $BiFeO_3$ crystals (1.77 pC/N). Besides, as illustrated in Fig. 5(a), under the equal mass of pressure sensing materials, the bulk $BiFeO_3$ based pressure sensor possessed less interparticle interface as compared to the sensor based on exfoliated thinner nanoplates. Therefore, the electric charge induced by external pressure in the sensor based on bulk $BiFeO_3$ crystals is mostly stored at the interface between the film and the electrodes, while the sensor based on $BiFeO_3$ nanoplates could have additional electric charges accumulated at the extra interfaces between thin layers, contributing to the enhanced capacitance [27, 43]. This is further demonstrated in Fig. 5(b) that the exfoliated $BiFeO_3$ exhibited the higher output capacitance than that of bulk $BiFeO_3$ on the basis of equal mass.

## 4 Conclusion

In summary, different from the commonly synthesized bulk $BiFeO_3$ crystals, thin-layered $BiFeO_3$ nanoplates were successfully prepared by a hydrothermal method followed by freeze-drying assisted liquid exfoliation process. The as-prepared $BiFeO_3$ nanoplates showed lateral sizes of 400–500 nm. The vital role of freeze-drying and the effect of liquid exfoliation solvent were also detailed. It is believed that the freeze-drying is the precondition of the whole fabrication process, which can generate internal stress to facilitate the subsequent solvent exfoliation. Besides, the methanol solvent with the suitable surface tension and relatively smaller molecule size can be more easily driven into the layers for maximizing the exfoliation effect. Compared with bulk $BiFeO_3$, the as-fabricated pressure sensor based on the $BiFeO_3$ nanoplates exhibited largely enhanced sensitivity with a wider working range of pressure, attributing to enhanced piezoelectric effect induced by the extra electrical charges generated at interlayer interfaces. We hope the adopted method for the fabrication of thin-layer $BiFeO_3$ could extend to the preparation of other non-van der Waals layered crystals for wide applications.

**Conflicts of interest** There are no conflicts to declare.

**Electronic supplementary materials** The online version contains supplementary material available at https://doi.org/10.1007/s11467-023-1301-7 and https://journal.hep.com.cn/fop/EN/10.1007/s11467-023-1301-7.

**Acknowledgements** This work was supported by the National Natural Science Foundation of China (Grant No. 51832001).

## References

1. L. Tao, K. Zhang, H. Tian, Y. Liu, D. Y. Wang, Y. Q. Chen, Y. Yang, and T. L. Ren, Graphene-paper pressure sensor for detecting human motions, *ACS Nano* 11(9), 8790 (2017)
2. L. Guan, A. Nilghaz, B. Su, L. Jiang, W. Cheng, and W.

Shen, Stretchable-fiber-confined wetting conductive liquids as wearable human health monitors, *Adv. Funct. Mater.* 26(25), 4511 (2016)
3. C. M. Boutry, L. Beker, Y. Kaizawa, C. Vassos, H. Tran, A. C. Hinckley, R. Pfattner, S. Niu, J. Li, J. Claverie, Z. Wang, J. Chang, P. M. Fox, and Z. Bao, Biodegradable and flexible arterial-pulse sensor for the wireless monitoring of blood flow, *Nat. Biomed. Eng.* 3(1), 47 (2019)
4. L. Li, J. Zheng, J. Chen, Z. Luo, Y. Su, W. Tang, X. Gao, Y. Li, C. Cao, Q. Liu, X. Kang, L. Wang, and H. Li, Flexible pressure sensors for biomedical applications: From *ex vivo* to *in vivo*, *Adv. Mater. Interfaces* 7(17), 2000743 (2020)
5. D. Kim, N. Lu, R. Ma, Y. S. Kim, R. H. Kim, S. Wang, J. Wu, S. M. Won, H. Tao, A. Islam, K. J. Yu, T. Kim, R. Chowdhury, M. Ying, L. Xu, M. Li, H. J. Chung, H. Keum, M. McCormick, P. Liu, Y. W. Zhang, F. G. Omenetto, Y. Huang, T. Coleman, and J. A. Rogers, Epidermal electronics, *Science* 333(6044), 838 (2011)
6. S. C. B. Mannsfeld, B. C. K. Tee, R. M. Stoltenberg, C. V. H. H. Chen, S. Barman, B. V. O. Muir, A. N. Sokolov, C. Reese, and Z. Bao, Highly sensitive flexible pressure sensors with microstructured rubber dielectric layers, *Nat. Mater.* 9(10), 859 (2010)
7. D. J. Lipomi, M. Vosgueritchian, B. C. K. Tee, S. L. Hellstrom, J. A. Lee, C. H. Fox, and Z. Bao, Skin-like pressure and strain sensors based on transparent elastic films of carbon nanotubes, *Nat. Nanotechnol.* 6(12), 788 (2011)
8. F. Fan, L. Lin, G. Zhu, W. Wu, R. Zhang, and Z. L. Wang, Transparent triboelectric nanogenerators and self-powered pressure sensors based on micropatterned plastic films, *Nano Lett.* 12(6), 3109 (2012)
9. Y. Ding, J. Yang, C. R. Tolle, and Z. Zhu, Flexible and compressible PEDOT: PSS@melamine conductive sponge prepared via one-step dip coating as piezoresistive pressure sensor for human motion detection, *ACS Appl. Mater. Interfaces* 10(18), 16077 (2018)
10. X. Shuai, P. Zhu, W. Zeng, Y. Hu, X. Liang, Y. Zhang, R. Sun, and C. Wong, Highly sensitive flexible pressure sensor based on silver nanowires-embedded polydimethylsiloxane electrode with microarray structure, *ACS Appl. Mater. Interfaces* 9(31), 26314 (2017)
11. K. Maity, S. Garain, K. Henkel, D. Schmeißer, and D. Mandal, Self-powered human-health monitoring through aligned PVDF nanofibers interfaced skin-interactive piezoelectric sensor, *ACS Appl. Polym. Mater.* 2(2), 862 (2020)
12. S. Xu, Y. Qin, C. Xu, Y. Wei, R. Yang, and Z. L. Wang, Self-powered nanowire devices, *Nat. Nanotechnol.* 5(5), 366 (2010)
13. L. Lin, Y. Xie, S. Wang, W. Wu, S. Niu, X. Wen, and Z. L. Wang, Triboelectric active sensor array for self-powered static and dynamic pressure detection and tactile imaging, *ACS Nano* 7(9), 8266 (2013)
14. T. Huang, S. Yang, P. He, J. Sun, S. Zhang, D. Li, Y. Meng, J. Zhou, H. Tang, J. Liang, G. Ding, and X. Xie, Phase-separation-induced PVDF/graphene coating on fabrics toward flexible piezoelectric sensors, *ACS Appl. Mater. Interfaces* 10(36), 30732 (2018)
15. M. Ha, S. Lim, J. Park, D. S. Um, Y. Lee, and H. Ko, Bioinspired interlocked and hierarchical design of ZnO nanowire arrays for static and dynamic pressure-sensitive electronic skins, *Adv. Funct. Mater.* 25(19), 2841 (2015)
16. Y. Kim, K. Y. Lee, S. K. Hwang, C. Park, S. W. Kim, and J. Cho, Layer-by-layer controlled perovskite nanocomposite thin films for piezoelectric nanogenerators, *Adv. Funct. Mater.* 24(40), 6262 (2014)
17. Y. Qi and M. C. McAlpine, Nanotechnology-enabled flexible and biocompatible energy harvesting, *Energy Environ. Sci.* 3(9), 1275 (2010)
18. H. Liu, J. Zhong, C. Lee, S. W. Lee, and L. Lin, A comprehensive review on piezoelectric energy harvesting technology: Materials, mechanisms, and applications, *Appl. Phys. Rev.* 5(4), 041306 (2018)
19. H. G. Yeo, T. Xue, S. Roundy, X. Ma, C. Rahn, and S. Trolier-McKinstry, Strongly (001) oriented bimorph PZT film on metal foils grown by *RF*-sputtering for wrist-worn piezoelectric energy harvesters, *Adv. Funct. Mater.* 28(36), 1801327 (2018)
20. J. Yi, L. Liu, L. Shu, Y. Huang, and J. F. Li, Outstanding ferroelectricity in sol–gel-derived polycrystalline $BiFeO_3$ films within a wide thickness range, *ACS Appl. Mater. Interfaces* 14(18), 21696 (2022)
21. J. Wang, J. B. Neaton, H. Zheng, V. Nagarajan, S. B. Ogale, B. Liu, D. Viehland, V. Vaithyanathan, D. G. Schlom, U. V. Waghmare, N. A. Spaldin, K. M. Rabe, M. Wuttig, and R. Ramesh, Epitaxial $BiFeO_3$ multiferroic thin film heterostructures, *Science* 299(5613), 1719 (2003)
22. J. Silva, A. Reyes, H. Esparza, H. Camacho, and L. Fuentes, $BiFeO_3$: A review on synthesis, doping and crystal structure, *Integr. Ferroelectr.* 126(1), 47 (2011)
23. M. Dai, Z. Wang, F. Wang, Y. Qiu, J. Zhang, C. Y. Xu, T. Zhai, W. Cao, Y. Fu, D. Jia, Y. Zhou, and P. A. Hu, Two-dimensional van der Waals materials with aligned in-plane polarization and large piezoelectric effect for self-powered piezoelectric sensors, *Nano Lett.* 19(8), 5410 (2019)
24. M. H. Lee, D. J. Kim, J. S. Park, S. W. Kim, T. K. Song, M. H. Kim, W. J. Kim, D. Do, and I. K. Jeong, High-performance lead-free piezoceramics with high Curie temperatures, *Adv. Mater.* 27(43), 6976 (2015)
25. K. Shimizu, H. Hojo, Y. Ikuhara, and M. Azuma, Enhanced piezoelectric response due to polarization rotation in cobalt-substituted $BiFeO_3$ epitaxial thin films, *Adv. Mater.* 28(39), 8639 (2016)
26. K. Shimizu, H. Hojo, Y. Ikuhara, and M. Azuma, Piezoelectric materials: Enhanced piezoelectric response due to polarization rotation in cobalt-substituted $BiFeO_3$ epitaxial thin films, *Adv. Mater.* 28(39), 8785 (2016)
27. P. Hu, L. Yan, C. Zhao, Y. Zhang, and J. Niu, Double-layer structured PVDF nanocomposite film designed for flexible nanogenerator exhibiting enhanced piezoelectric output and mechanical property, *Compos. Sci. Technol.* 168, 327 (2018)
28. K. N. Duerloo, M. T. Ong, and E. J. Reed, Intrinsic piezoelectricity in two-dimensional materials, *J. Phys. Chem. Lett.* 3(19), 2871 (2012)
29. Liu, G. D. Zhao, T. Hu, L. Bellaiche, and W. Ren, Structural and magnetic properties of two-dimensional

layered $BiFeO_3$ from first principles, *Phys. Rev. B* 103, 081403 (2021)
30. H. Yan, H. Deng, N. Ding, J. He, L. Peng, L. Sun, P. Yang, and J. Chu, Influence of transition elements doping on structural, optical and magnetic properties of $BiFeO_3$ films fabricated by magnetron sputtering, *Mater. Lett.* 111, 123 (2013)
31. X. Zhang, J. Deng, J. Yan, Y. Song, Z. Mo, J. Qian, X. Wu, S. Yuan, H. Li, and H. Xu, Cryo-mediated liquid-phase exfoliated 2D BP coupled with 2D $C_3N_4$ to photodegradate organic pollutants and simultaneously generate hydrogen, *Appl. Surf. Sci.* 490, 117 (2019)
32. H. Wang, W. Lv, J. Shi, H. Wang, D. Wang, L. Jin, J. Chao, P. A. van Aken, R. Chen, and W. Huang, Efficient liquid nitrogen exfoliation of $MoS_2$ ultrathin nanosheets in the pure 2H phase, *ACS Sustain. Chem. & Eng.* 8(1), 84 (2020)
33. Y. Wang, Y. Liu, J. Zhang, J. Wu, H. Xu, X. Wen, X. Zhang, C. S. Tiwary, W. Yang, R. Vajtai, Y. Zhang, N. Chopra, I. N. Odeh, Y. Wu, and P. M. Ajayan, Cryo-mediated exfoliation and fracturing of layered materials into 2D quantum dots, *Sci. Adv.* 3(12), 1701500 (2017)
34. M. Abroodi, A. Bagheri, and B. M. Razavizadeh, Surface tension of binary and ternary systems containing monoethanolamine (MEA), water and alcohols (methanol, ethanol, and isopropanol) at 303.15 K, *J. Chem. Eng. Data* 65(6), 3173 (2020)
35. S. Cesur, M. E. Cam, F. S. Sayin, and O. Gunduz, Electrically controlled drug release of donepezil and $BiFeO_3$ magnetic nanoparticle-loaded PVA microbubbles/nanoparticles for the treatment of Alzheimer's disease, *J. Drug Deliv. Sci. Technol.* 67, 102977 (2022)
36. H. Ding, S. T. Khan, S. Zeng, and L. Sun, Exfoliation of nanosized α-zirconium phosphate in methanol, *Inorg. Chem.* 60(11), 8276 (2021)
37. K. Jonnalagadda, S. W. Cho, I. Chasiotis, T. Friedmann, and J. Sullivan, Effect of intrinsic stress gradient on the effective mode-I fracture toughness of amorphous diamond-like carbon films for MEMS, *J. Mech. Phys. Solids* 56(2), 388 (2008)
38. K. Park, J. H. Son, G. T. Hwang, C. K. Jeong, J. Ryu, M. Koo, I. Choi, S. H. Lee, M. Byun, Z. L. Wang, and K. J. Lee, Highly-efficient, flexible piezoelectric PZT thin film nanogenerator on plastic substrates, *Adv. Mater.* 26(16), 2514 (2014)
39. A. Barzegar, D. Damjanovic, and N. Setter, Analytical modeling of the apparent $d_{33}$ piezoelectric coefficient determined by the direct quasistatic method for different boundary conditions, *IEEE Trans. Ultrason. Ferroelectr. Freq. Control* 52(11), 1897 (2005)
40. J. Dong and G. Ouyang, Edge effect on the piezoelectric characteristics of rectangular-shaped monolayer $MSe_2$ (M = Cr, Mo, W) nanosheets, *J. Phys. D Appl. Phys.* 54(23), 235502 (2021)
41. Z. Zhu, A. Zhang, G. Ouyang, and G. Yang, Edge effect on band gap shift in Si nanowires with polygonal cross-sections, *Appl. Phys. Lett.* 98(26), 263112 (2011)
42. J. Dong and G. Ouyang, Edge effect on the piezoelectric characteristics of rectangular-shaped monolayer $MSe_2$ (M = Cr, Mo, W) nanosheets, *J. Phys. D: Appl. Phys.* 54(23), 235502 (2021)
43. Y. Lee, J. Park, S. Cho, Y. E. Shin, H. Lee, J. Kim, J. Myoung, S. Cho, S. Kang, C. Baig, and H. Ko, Flexible ferroelectric sensors with ultrahigh pressure sensitivity and linear response over exceptionally broad pressure range, *ACS Nano* 12(4), 4045 (2018)